Molecular Bases of Disease:

Lipocalin-2 Induces Cardiomyocyte Apoptosis by Increasing Intracellular Iron Accumulation

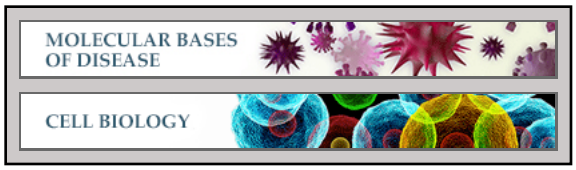

Guoxiong Xu, JinHee Ahn, SoYoung Chang, Megumi Eguchi, Arnaud Ogier, SungJun Han, YoungSam Park, ChiYoung Shim, YangSoo Jang, Bo Yang, Aimin Xu, Yu Wang and Gary Sweeney

J. Biol. Chem. 2012, 287:4808-4817.
doi: 10.1074/jbc.M111.275719 originally published online November 22, 2011

THE JOURNAL OF BIOLOGICAL CHEMISTRY VOL. 287, NO. 7, pp. 4808–4817, February 10, 2012

Lipocalin-2 Induces Cardiomyocyte Apoptosis by Increasing Intracellular Iron Accumulation*[S]

Received for publication, June 24, 2011, and in revised form, November 8, 2011 Published, JBC Papers in Press, November 23, 2011, DOI 10.1074/jbc.M111.275719

Guoxiong Xu[‡], JinHee Ahn[‡], SoYoung Chang[‡], Megumi Eguchi[‡§1], Arnaud Ogier[¶], SungJun Han[‖], YoungSam Park[‖], ChiYoung Shim[**], YangSoo Jang[**], Bo Yang[‡‡], Aimin Xu[‡‡], Yu Wang[‡‡], and Gary Sweeney[‡§2]

From the [‡]Diabetes Group, [¶]Toxicity Group, and [‖]Drug Biology Group, Institut Pasteur Korea, Seongnam, Gyeonggi 463-400, South Korea, the [**]Department of Cardiology, Yonsei University College of Medicine, Seoul 120-752, South Korea, the [‡‡]Department of Pharmacology, University of Hong Kong, Pokfulam, Hong Kong, and the [§]Department of Biology, York University, Toronto, Ontario M3J 1P3, Canada

Background: The proinflammatory adipokine lipocalin-2 is associated with obesity-related complications, such as heart failure.
Results: Lipocalin-2 induces cardiomyocyte apoptosis via elevating intracellular iron levels and mediates detrimental effects on cardiac function.
Conclusion: Lipocalin-2 is an important mediator of cardiac remodeling.
Significance: Regulation of cardiomyocyte apoptosis by lipocalin-2, and the mechanistic role of changes in intracellular iron, may contribute to the pathogenesis of obesity-related heart failure.

Our objective was to determine whether lipocalin-2 (Lcn2) regulates cardiomyocyte apoptosis, the mechanisms involved, and the functional significance. Emerging evidence suggests that Lcn2 is a proinflammatory adipokine associated with insulin resistance and obesity-related complications, such as heart failure. Here, we used both primary neonatal rat cardiomyocytes and H9c2 cells and demonstrated for the first time that Lcn2 directly induced cardiomyocyte apoptosis, an important component of cardiac remodeling leading to heart failure. This was shown by detection of DNA fragmentation using TUNEL assay, phosphatidylserine exposure using flow cytometry to detect annexin V-positive cells, caspase-3 activity using enzymatic assay and immunofluorescence, and Western blotting for the detection of cleaved caspase-3. We also observed that Lcn2 caused translocation of the proapoptotic protein Bax to mitochondria and disruption of mitochondrial membrane potential. Using transient transfection of GFP-Bax, we confirmed that Lcn2 induced co-localization of Bax with MitoTracker® dye. Importantly, we used the fluorescent probe Phen Green SK to demonstrate an increase in intracellular iron in response to Lcn2, and depleting intracellular iron using an iron chelator prevented Lcn2-induced cardiomyocyte apoptosis. Administration of recombinant Lcn2 to mice for 14 days increased cardiomyocyte apoptosis as well as an acute inflammatory response with compensatory changes in cardiac functional parameters. In conclusion, Lcn2-induced cardiomyocyte apoptosis is of physiological significance and occurs via a mechanism involving elevated intracellular iron levels and Bax translocation.

Cardiovascular disease is the leading cause of death worldwide, and individuals with obesity and type 2 diabetes have an increase in prevalence for cardiovascular morbidity and mortality (1–3). Heart failure is one example, but mechanisms of obesity- and diabetes-induced heart disease are multifaceted and remain to be defined clearly (4). A potential mechanism may be changes in cardiac remodeling as a result of altered circulating adipokine and cytokine profiles (5). Lipocalin-2 (Lcn2,[3] also often termed neutrophil gelatinase-associated lipocalin (NGAL) or oncogene 24p3), is a small, secreted adipokine and belongs to a diverse family of lipocalins that has the characteristics of binding and transporting small molecules such as retinoid, fatty acid, steroid, and iron (6–9). Recent studies show that Lcn2 is a proinflammatory marker associated with insulin resistance and obesity-related metabolic disorders (10–14). An increase of Lcn2 expression in adipose tissue is observed in various experimental models of obesity and in obese humans (11, 15, 16). It was suggested that Lcn2 may mediate the innate immune responses in the pathogenesis of heart failure (17–20). Lcn2 expression is significantly augmented in patients with coronary heart disease and myocardial infarction (12, 21). Plasma Lcn2 was increased after carotid artery injury in rats (22) and in a heterotopic mouse transplanted heart after ischemia/reperfusion (23).

Cardiomyocyte apoptosis can play a critical role in the progression of heart failure. For example, in patients with end-stage cardiomyopathy in dilated and ischemic heart disease, hypertrophic heart disease and arrhythmogenic right ventricular dysplasia, loss of cardiomyocytes due to apoptosis can be observed that leads to the progression of cardiac dysfunction, ultimately heart failure (24–27). Lcn2 has been implicated in

* This work was supported by National Research Foundation of Korea Grant 2010-0012009 (to G. S.) and by Collaborative Research Fund HKU 2/07C and 4/HKU/10C from the Research Grants Council of Hong Kong (to A. X. and Y. W.).
[S] This article contains supplemental Figs. S1–S4.
[1] Recipient of Heart and Stroke Foundation of Canada postgraduate studentship award.
[2] To whom correspondence should be addressed: Institut Pasteur Korea, 696 Sampyung-dong, Bundang-gu, Sungnam, Gyeonggi 463-400, Korea. Tel.: 82-31-8018-8002; Fax: 82-31-8018-8011; E-mail: gary@ip-korea.org.
[3] The abbreviations used are: Lcn2, lipocalin-2; AV, annexin V; 2′-DPD, 2,2′-dipyridyl; HBSS, Hanks' buffered salt solution; PG-SK, Phen Green SK; PI, propidium iodide; TMRE, tetramethylrhodamine ethylester.

the regulation of cell death in various cell types (28–31), although whether Lcn2 directly regulates cardiomyocyte apoptosis remains unknown. It has been shown that changes in intracellular iron content can mediate apoptosis in a variety of cell types (32–35). Furthermore, iron overload is associated with cardiomyopathy involving apoptosis and fibrosis leading to heart failure (36–39). Because Lcn2 has the capability to bind iron (40–43), we hypothesized that the alteration of intracellular iron levels is an important mechanism in Lcn2-induced apoptosis. This study therefore set out to analyze the role of Lcn2 on apoptosis at cellular and molecular levels, which may lead to better understanding of the pathophysiological role of Lcn2 in cardiomyopathy.

EXPERIMENTAL PROCEDURES

General Methods—The isolation and primary culture of neonatal rat ventricular myocytes were described by us previously (44). H9c2 cells were cultured as previously described (50). Wild-type C57BL/6J mice were injected with 200 μg/120 μl Lcn2 per mouse daily for up to 14 days. Heart function was assessed using Vevo2100 system (VisualSonics, Toronto, ON, Canada) equipped with MS550D transducer. All procedures were approved by Institut Pasteur Korea Institutional Animal Care and Use Committee. We produced recombinant mouse Lcn2 in a bacterial expression system and confirmed it by SDS-PAGE and mass spectrometry analysis as described previously (11, 13).

Measures of Apoptosis—Apoptotic cells were quantified by terminal deoxyribonucleotide transferase-mediated dUTP nick end-labeling (TUNEL) assay (*In Situ* Cell Death Detection Kit, Fluorescein, Roche Diagnostics) following the manufacturer's suggested protocol. To quantify the number of apoptotic cells further, flow cytometry using the FITC Annexin V Apoptosis Detection Kit I (BD Biosciences) was applied following the manufacturer's suggested protocol. Caspase-3 activity was measured using a Caspase-3 Colorimetric Assay kit (Abcam, Cambridge, UK) according to the manufacturer's instructions. Immunofluorescence staining of endogenous cleaved caspase-3 and Bax was performed in 96-well or 6-well plates, respectively. The nuclei were stained with DAPI. Alexa Fluor 488 and 594 secondary antibodies were from Invitrogen, and rabbit anti-N-terminal Bax (N-20) was from Santa Cruz Biotechnology. The mitochondrial membrane potential ($\Delta\Psi_m$) was determined using MitoShift assay as described previously (46) by staining of mitochondria with tetramethylrhodamine ethylester (TMRE) dye (Invitrogen). From *in vivo* studies, the heart was then removed and washed with PBS to wash out blood from the chambers. Thin sections (5 μm) from frozen heart embedded in OCT-compound were prepared. Apoptosis was assessed by TUNEL assay with an *in situ* cell death detection kit as described above and macrophage infiltration by CD68 staining.

Real-time Analysis of GFP-Bax Translocation—Transient transfection was performed in 96-well plate. Plasmid pEGFP-Bax was obtained from Dr. Hsu (Medical University of South Carolina) (48). Mitochondrial staining was performed using MitoTracker® Mitochondrion-selective Probes (MitoTracker® Red CMXRos; Molecular Probers). After transient transfection and Lcn2 treatment, cells were incubated with 25 nM MitoTracker® dye for 15 min, followed by Hoechst 33342 (Invitrogen) staining for another 10 min to stain the nuclei. Bax translocation was examined by real-time imaging using LSM5 confocal microscope (Carl Zeiss Microlmaging) with 63× (NA: 1.4) oil-immersion objective.

Western Blot Analysis—Cell lysates were prepared by washing cell monolayers with PBS and lysing in 1× Cell Lysis buffer (Cell Signaling Technology) containing phosphatase inhibitors and protease inhibitor mixture (Sigma). Equal protein amounts were separated by SDS-PAGE and transferred to a polyvinylidene difluoride membrane (Immobilon-P; Millipore Corp.). The following antibodies were used: rabbit anti-caspase-3, anti-cleaved caspase-3 (Asp-175), anti-total Bax, anti-β-actin, affinity-purified goat anti-rabbit IgG HRP, and affinity-purified horse anti-mouse IgG HRP (all from Cell Signaling Technology).

Measurement of Intracellular Phen Green SK-chelatable Iron Level and Image Analysis—Intracellular iron levels were measured using the fluorescent probe Phen Green SK (PG-SK; Invitrogen), essentially as described previously (49). For saturating the intracellular iron pool as a positive control, cells were treated with 100 μM ferrous sulfate ($FeSO_4$; Sigma) for 10 min. As a negative control, cells were incubated with a 5 mM concentration of the well characterized membrane-permeable iron chelator 2,2′-dipyridyl (2′-DPD, Sigma). After washing with Hanks' buffered salt solution (HBSS, pH 7.3), the cells were incubated with 10 μM PG-SK in HBSS at 37 °C for 10 min. After quickly washing with HBSS, the cells were incubated with Hoechst 33342 to stain the nuclei for 10 min, followed by 4% paraformaldehyde fixation. Fluorescence images were then recorded automatically by a confocal microplate imaging reader (Evotec Technologies OPERA™; PerkinElmer Life Sciences) at excitation 405 and 488 nm and emission 420 and 520 nm. We segmented cell by cell using in-house software allowing us to quantify the amount of green fluorescence in the cytoplasm. Both nuclei and cytoplasm were detected with intensity-independent well to well K-mean-based algorithm. The collected data (one point/cell) were analyzed with Spotfire™ software.

Iron Chelation and Supplementation—To chelate iron, cells were incubated in serum-free medium for 1 h followed by pretreatment with different dose of 2′-DPD in DMEM/0.2% FBS for 20 min. For saturating intracellular iron pool as a positive control, cells were treated with 100 μM $FeSO_4$ for 24 h. After treatment of 2 μg/ml Lcn2 in DMEM/0.2% FBS in the presence of 2′-DPD for 24 h, the cells were fixed with 4% paraformaldehyde and permeated with 0.1% Triton X-100. After blocking with 10% goat serum in PBS for 30 min, cells were incubated with anti-cleaved caspase-3 (Asp-175, 1:100 dilution) or anti-N terminus of Bax (1:200 dilution) in blocking solution for 2 h, followed by incubation with secondary anti-rabbit Alexa Fluor 488 or 594 antibodies (1:200 dilution). After the nuclei were stained with Hoechst 33342, the images were taken by a confocal microscopy. The number of positive cells over total cells was determined from randomly selected fields.

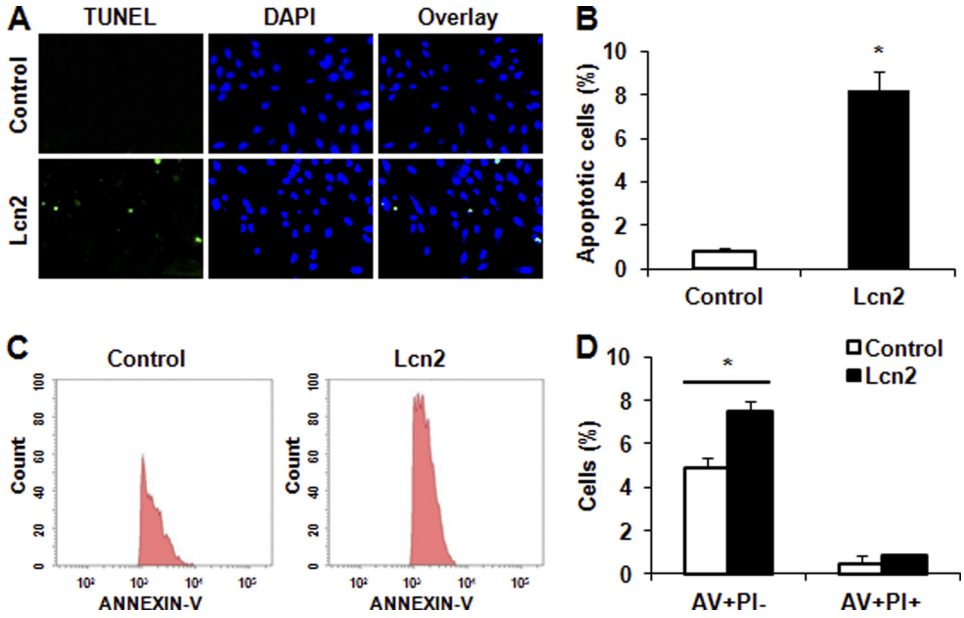

FIGURE 1. **Determination of apoptotic cells after Lcn2 treatment.** *A*, apoptotic cells were examined using TUNEL assay for DNA fragmentation. H9c2 cells were photographed by fluorescence microscopy (magnification, ×20) at 48 h after 2 μg/ml Lcn2 treatment. Cells treated with buffer not containing Lcn2 (*Control*) were used for comparison. TUNEL-positive nuclei are shown in *green*, total nuclei stained with DAPI in *blue*. *B*, quantitative analysis (percentage of apoptotic cells *versus* total) is shown in histogram (*, $p < 0.01$). *C*, after double staining, the AV^+ and PI^+ cells were analyzed by flow cytometry (*left panel*, control cells; *right panel*, Lcn2-treated cells). *D*, quantitative determination of data from FACS analysis showing treatment of Lcn2 (1 μg/ml) for 16 h elicited a significant increase in the number of cells undergoing apoptosis (AV^+/PI^-) ($n = 3$; *, $p < 0.05$).

Statistical Analysis—Data from experiments were expressed as percentage of the value or arbitrary unit from control *versus* Lcn2 treatment. *Bars* in figures represent mean ± S.E. values determined from at least three independent samples or experiments. Statistical analysis for assessing significant differences among multiple groups was done with one-way ANOVA, followed by a Tukey-Kramer multiple comparisons test (Graph Pad InStat Software; Graph Pad Inc., San Diego, CA). For comparison between two groups, Student's *t* test was used. Differences were considered significant at values of $p < 0.05$.

RESULTS

Lcn2 Induces Cardiomyocyte Apoptosis—We first used a TUNEL assay to detect DNA fragmentation and showed that more apoptotic cells were evident after treatment of H9c2 cells with 2 μg/ml recombinant Lcn2 for 48 h (Fig. 1*A*). We used 1–5 μg/ml Lcn2 in this study based upon preliminary experiments and published data (13). Quantitative analysis of TUNEL-positive cells demonstrated a significant increase of almost 8-fold in apoptotic cells after Lcn2 treatment compared with untreated control (Fig. 1*B*). This was also observed in primary neonatal cardiomyocytes (Fig. S1). Because the exposure of phosphatidylserine on the outer leaflet of the plasma membrane is one of the earliest features of apoptosis, we used annexin V (AV) to detect phosphatidylserine in intact cells. Simultaneously, cell-permeable propidium iodide (PI) was used to stain the nucleus, and apoptotic cells were analyzed further using this double staining with AV and PI, followed by flow cytometry. An increased population of AV^+/PI^- cells, indicating an early stage of apoptotic cells, was observed after 1 μg/ml Lcn2 treatment for 16 h (Fig. 1*C*). After quantification of data from three independent experiments, we found that the number of AV^+/PI^- cells, but not AV^+/PI^+, was significantly increased after Lcn2 treatment compared with untreated controls (Fig. 1*D*).

Lcn2 Increases Caspase-3 Cleavage and Activity—We next investigated whether caspase-3 cleavage is increased by Lcn2. First, H9c2 cells were treated with 1 μg/ml Lcn2 for 16 h before fixation and immunofluorescent detection of cleaved caspase-3 using a specific antibody (Asp-175). We found that Lcn2 induced cleavage of caspase-3 (Fig. 2*A*), and quantitative analysis showed that the number of cleaved caspase-3-positive cells was significantly increased by >8-fold (Fig. 2*B*). Importantly, the increased cleaved caspase-3 was also observed in neonatal rat cardiomyocytes exposed to 1 and 2 μg/ml Lcn2 for 24 h (Fig. 2, *C* and *D*). Lcn2-induced caspase-3 cleavage was further confirmed by Western blotting using an antibody against the cleaved form of caspase-3. We observed that the level of cleaved form (17 kDa) of caspase-3 was significantly increased in H9c2 cells after Lcn2 treatment (Fig. 2, *E* and *F*). We then directly measured the activity of caspase-3 using an assay based on cleavage of a fluorogenic substrate and found that the activity of caspase-3 was significantly increased in cells exposed to 2 μg/ml Lcn2 for 24 h (Fig. 2*G*).

Lcn2 Leads to Disruption of Mitochondrial Membrane Potential—The disruption of mitochondrial membrane potential is characteristic of intrinsic cellular apoptosis and plays an important role in the activation of caspase-3. The integrity of the mitochondrial membrane was measured here by MitoShift assay using TMRE dye. In control cells, the dye was located in the mitochondria and appeared mainly as punctate red fluorescence (Fig. 3). However, the dye relocates upon disruption of mitochondrial membrane and appeared as more diffuse and weaker fluorescence in the cytoplasm of cells after 1, 2, and 4

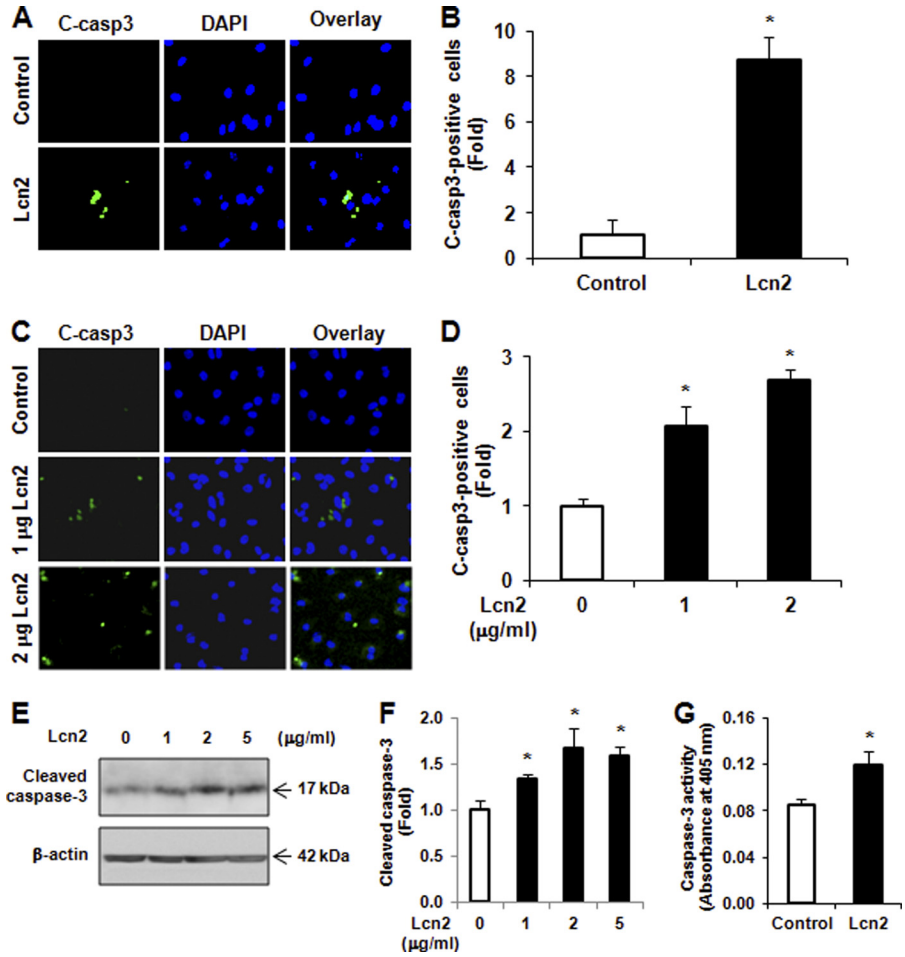

FIGURE 2. **Detection of cleaved caspase-3 and its activity.** *A*, H9c2 cells were treated without (*Control*) or with 1 μg/ml Lcn2 for 16 h before immunofluorescent detection (magnification, ×20) of cleaved caspase-3 (*green*), and nuclei were strained with DAPI (*blue*). *B*, number of cleaved caspase-3-positive cells was counted from six randomly selected fields in each individual experiment, and at least three independent experiments were performed and analyzed (*, $p < 0.01$). *C* and *D*, as explained for *A* and *B*, except neonatal rat cardiomyocytes exposed to 1 or 2 μg/ml Lcn2 for 48 h were used (*, $p < 0.05$). *E* and *F*, cells were treated with 0, 1, 2, or 5 μg/ml Lcn2 for 24 h, and total protein was extracted and subjected to Western blotting using an antibody recognizing cleaved caspase-3. β-Actin was used as a loading control. A representative blot is shown (*E*), and $n = 3$ experiments are quantitated in *F* (*, $p < 0.05$). *G*, H9c2 cells were treated with 2 μg/ml Lcn2 for 24 h, and cell lysates were assayed for caspase-3 activity ($n = 3$; *, $p < 0.05$).

μg/ml Lcn2 treatment for 24 (data not shown) and 48 h (Fig. 3*A*). Quantitative analysis of fluorescence units of TMRE demonstrated a significant decrease in Lcn2-treated cells (Fig. 3*B*). A similar disruption of mitochondrial membrane potential was also observed in primary neonatal cardiomyocytes (Fig. S2, *A* and *B*).

Lcn2 Stimulates Bax Translocation to Mitochondria—Bax is an important proapoptotic factor involved in the intrinsic pathway of apoptosis and increases the mitochondrial membrane permeability by translocating and integrating into the membrane. Here, we examined translocation of Bax by first using an antibody against an epitope in the N-terminal domain of Bax which is normally obscured and only exposed as Bax changes its conformation when it integrates into the membrane of mitochondria (50). We detected an increase in the endogenous active form of Bax in H9c2 cells after 1 μg/ml Lcn2 treatment for 16 h (Fig. 4*A*). In untreated cells, few or no N-terminal Bax immunofluorescence signals were observed. Lcn2-induced Bax translocation was also observed in neonatal rat cardiomyocytes after the treatment of 1 and 2 μg/ml Lcn2 for 48 h (Fig. 4*B*). To further examine and confirm the translocation of Bax, we transiently transfected GFP-Bax into H9c2 cells followed by 1 or 2 μg/ml Lcn2 treatment for 24 h. Mitochondria were then stained in living cells with MitoTracker® dye, allowing analysis of co-localization with GFP-Bax using confocal microscopy. We observed a higher extent of GFP-Bax co-localizing with MitoTracker® upon Lcn2 treatment (Fig. 4*C*). In control, GFP-transfected, cells distinct signals for MitoTracker® dye and GFP were observed (Fig. 4*C*).

Lcn2 Alters Intracellular Iron Levels, Leading to Increase in Cleaved Caspase-3—It has been shown that iron can mediate apoptosis in a variety of cell types, and because Lcn2 has the capability of binding to iron we next examined intracellular iron levels in H9c2 cells using the cell-permeable fluorescent probe PG-SK. This probe can be quenched by binding intracellular free iron. Cell treatment with $FeSO_4$ and 2′-DPD was used as positive and negative controls and clearly showed decreased and increased levels of fluorescence, respectively (Fig. 5*A*). Interestingly, we found by observing segmented confocal images that the signal of PG-SK fluorescence was attenuated after 2 μg/ml Lcn2 treatment for 24 h (Fig. 5*A*), indicating an increase in the level of intracellular iron. We also treated cells

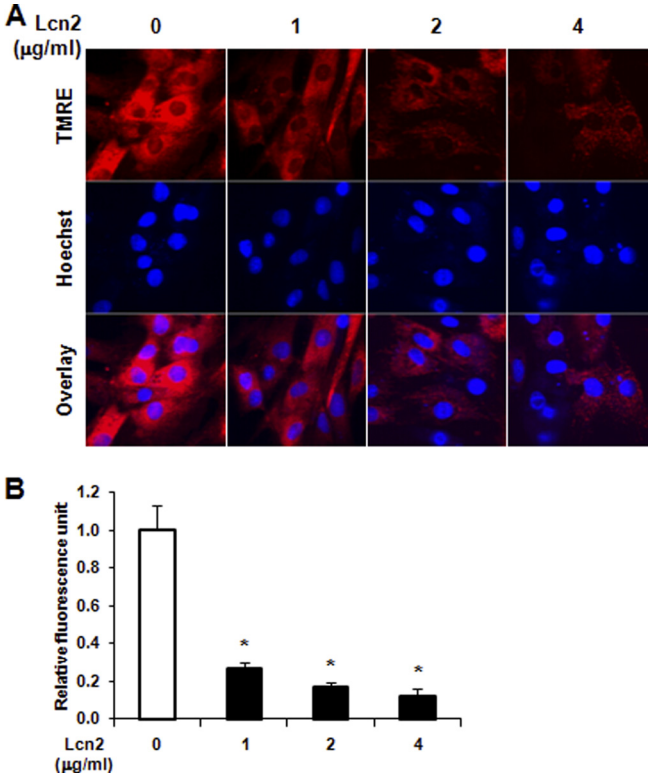

FIGURE 3. **Assessment of mitochondrial membrane potential in H9c2 cells.** *A*, cells were treated with 1, 2, and 4 μg/ml Lcn2 for 48 h and analyzed by confocal microscopy (magnification, ×40) using TMRE dye, with total nuclei identified using Hoechst 33342. *B*, quantitative analysis of relative fluorescence intensity is shown ($n = 4$; *, $p < 0.01$).

with 2′-DPD (5 mM) for 10 min to chelate intracellular iron and found a strong increase in PG-SK fluorescence (Fig. S3). To quantitate this phenomenon we used an automated confocal reader together with Spotfire software analysis to assess PG-SK fluorescence in a large population of single cells. Fig. 5*B* displays the range of intracellular iron levels (mean PG-SK fluorescence) in control cells (*red*) and shows that there was a trend of decreased fluorescence in a significant number of Lcn2-treated cells (*green*). A small number of $FeSO_4$-treated cells (*yellow*) were used to validate this quantitative approach. Fig. 5*C* shows a representative analysis where the number of cells analyzed in each treatment is shown (*Count*), and the median fluorescent intensity was changed from 2859 (*Control*) to 1754 after treatment of cells with Lcn2. The number of outliers in each case is very small relative to the total number of cells analyzed (~1%). These data indicate that Lcn2 increased intracellular iron in cardiomyocytes overall, but not in all cells, which led us to determine whether there was a direct functional significance of this change. Using immunofluorescent staining with an antibody specific to cleaved caspase-3 in combination with PG-SK analysis, we confirmed that individual cells exhibiting decreased PG-SK fluorescence after Lcn2 treatment also showed an increase in cleaved caspase-3 (Fig. 6*A*). Upon temporal analysis of treatment with Lcn2 up to 24 h, we observed that changes in PG-SK fluorescence preceded an increase in cleaved caspase-3. This suggests that changes in intracellular iron may mediate subsequent apoptotic events. To confirm the mechanistic role of altered intracellular iron levels we next

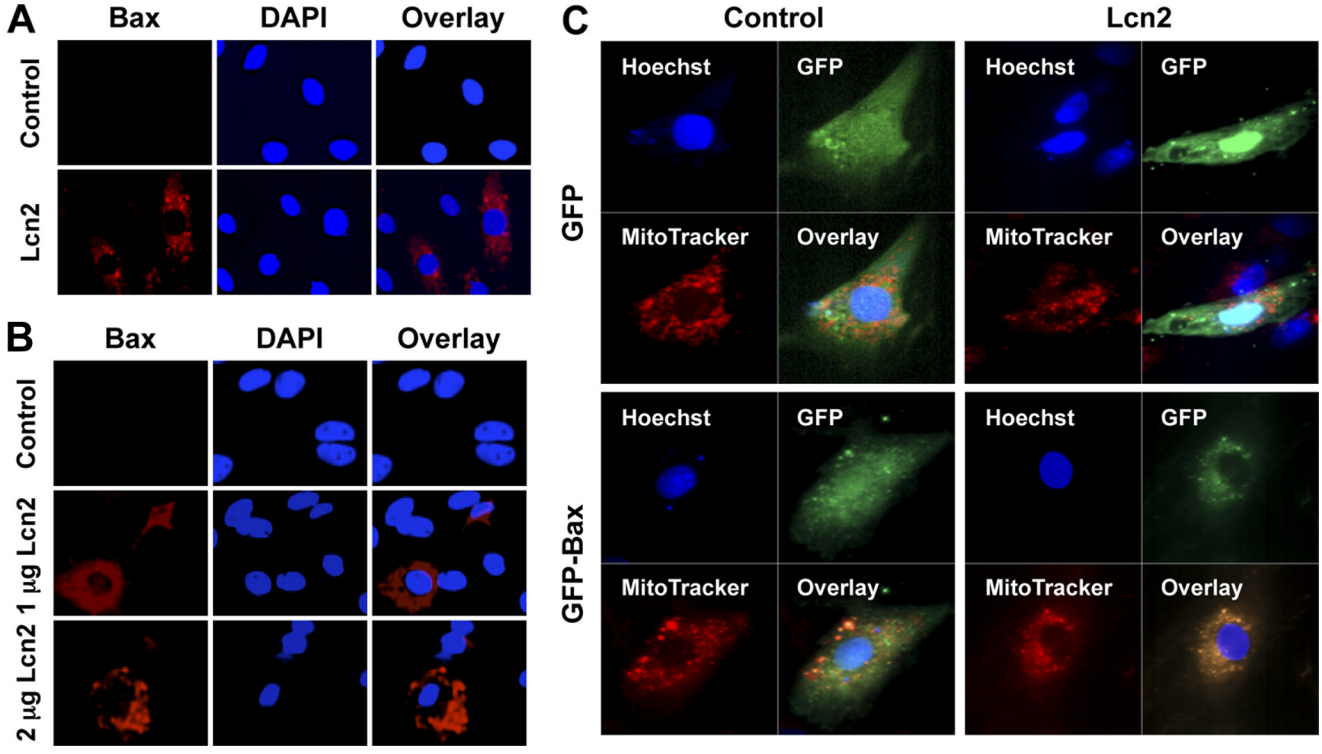

FIGURE 4. **Detection of Bax translocation to mitochondrial membrane in response to Lcn2.** *A* and *B*, H9c2 cells (*A*) or primary cardiomyocytes (*B*) were treated with or without 1 or 2 μg/ml Lcn2 for 16 h followed by detection of N-terminal Bax epitope (*red*), which is only detectable once the protein is inserted in mitochondrial membrane, with nuclei detected using DAPI. Representative images of $n = 3$ experiments in each case are shown (magnification, ×20). *C*, H9c2 cells were transiently transfected with GFP-Bax or GFP (*Control*), followed by treatment with 2 μg/ml Lcn2 for 24 h. Mitochondria in live cells were identified using MitoTracker®, in combination with nuclei staining using Hoechst 33342 and examined by confocal microscopy (magnification, ×63). Representative images of $n = 3$ experiments are shown.

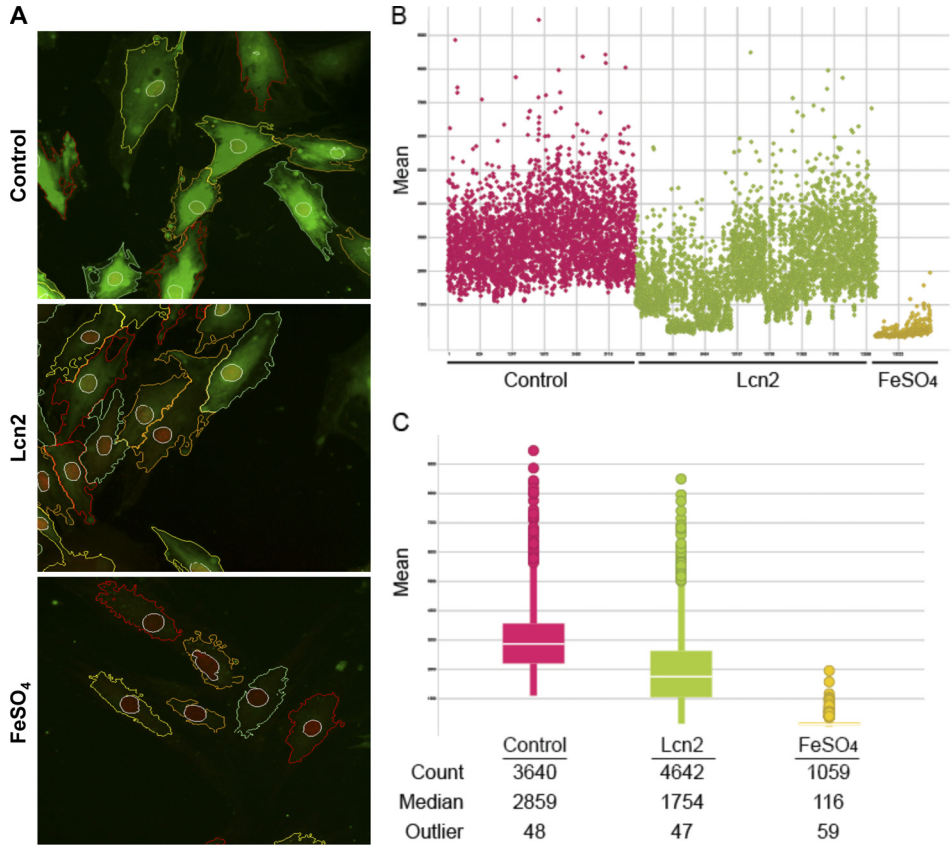

FIGURE 5. **Determination of intracellular iron level using PG-SK.** *A*, intracellular free iron levels were monitored in H9c2 cells treated with 2 μg/ml Lcn2 for 24 h, using the cell-permeable fluorescent dye PG-SK, which is quenched upon binding iron. Treatment of $FeSO_4$ (100 μM) was used as positive control. The images shown are representative segmented images from automated confocal microscopy analysis. *B*, intensity of fluorescent signal/cell was measured and analyzed cell by cell in populations treated without or with Lcn2 or $FeSO_4$, and distribution of values is shown here. *C*, quantitative analysis of cell by cell data is shown for each condition with number of cells, median fluorescence, and number of outlying values shown.

examined iron-induced apoptosis directly by detecting cleaved caspase-3 using Western blotting. We found that the treatment of 100 μM $FeSO_4$ indeed resulted in an increase of cleaved caspase-3 in a time-dependent manner in H9c2 cells (Fig. 6*B*). Conversely, when we depleted intracellular iron in neonatal rat cardiomyocytes using the iron chelator 2′-DPD we observed that Lcn2-induced caspase-3 cleavage was attenuated (Fig. 6*C*). This phenomenon was further confirmed by showing that 2′-DPD pretreatment decreased the ability of Lcn2 to cause Bax translocation to mitochondria (Fig. 6*D*). The involvement of altered intracellular iron levels in apoptosis was also observed in H9c2 cells (Fig. S4).

Lcn2 Plays Important Physiological Role in Inducing Cardiomyocyte Apoptosis—We next performed studies in mice that were administered recombinant Lcn2, and we observed that after 14 days an increased number of apoptotic cells were detected in heart sections by TUNEL and DAPI staining (Fig. 7*A*). The number of TUNEL-positive cells in wild-type mice was, as expected, very low (<0.5%), and this was increased significantly to almost 4% after 14 days of Lcn2 treatment (Fig. 7*B*). The circulating Lcn2 level was confirmed by ELISA to be increased at 14 days of treatment to (7.19 ± 0.92 μg/ml compared with 3.98 ± 0.18 μg/ml in PBS-injected mice). We also examined macrophage infiltration (CD68 staining) in heart sections as a measure of inflammation and found that Lcn2 induced an inflammatory response in the heart after 14 days administration (Fig. 7, *C* and *D*). Analysis of cardiac structure and function by echocardiography at 14 days indicated that Lcn2-treated mice showed a trend toward decreased left ventricular end systolic and diastolic volumes and increases in fractional shortening, E′ velocity, heart rate, and cardiac output (Table 1).

DISCUSSION

Emerging data indicate that circulating levels of Lcn2 correlate positively with various aspects of the metabolic syndrome (10). Work to date has focused principally on the proinflammatory and metabolic effects of Lcn2 (11, 13, 51–53), yet less is known regarding cardiovascular effects. Several studies have now shown that Lcn2 was elevated during ischemia-reperfusion processes and in coronary heart disease and myocardial infarction (12, 20, 21, 23). Here, we analyzed the effect of Lcn2 on cardiomyocyte apoptosis, an important component of cardiac remodeling leading to heart failure (24, 25).

Our data using FACS analysis of annexin V binding to phosphatidylserine, TUNEL staining, and various measures of caspase-3 activation clearly demonstrate that recombinant Lcn2 induced apoptosis in primary neonatal cardiomyocytes and H9c2 cells. Because this is a novel observation and little is known about Lcn2 signaling we next investigated potential mechanisms responsible for Lcn2-induced apoptosis. Our studies uncovered an initially unexpected and novel mecha-

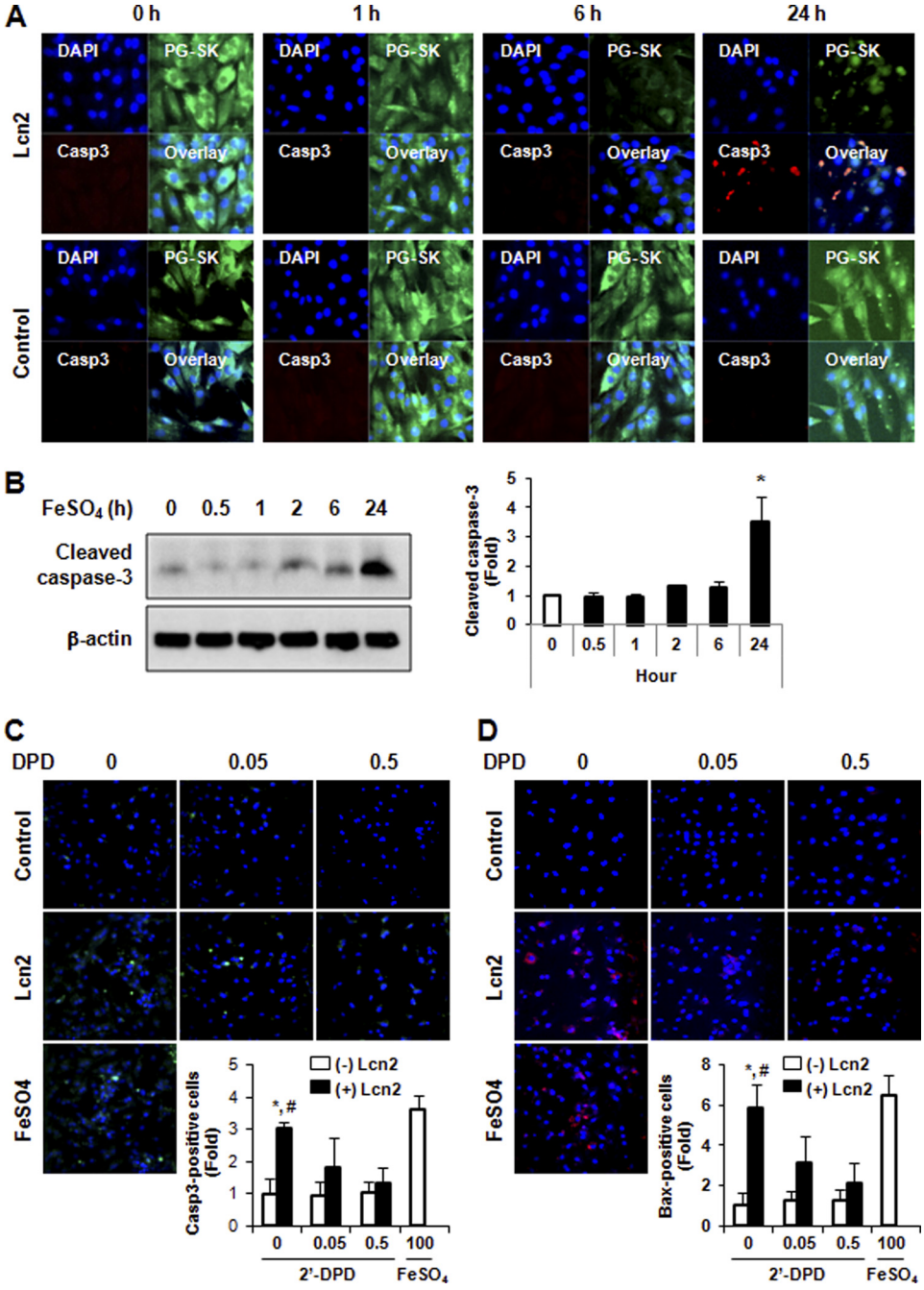

FIGURE 6. **Involvement of changing intracellular iron levels in apoptosis.** *A*, intracellular iron was detected by PG-SK and cleaved caspase-3 by immunofluorescence to demonstrate that cells within a population responding to Lcn2 (2 μg/ml, up to 24 h) with increased intracellular iron also exhibited more cleaved caspase-3 detection in H9c2 cells. Representative images of $n = 4$ experiments are shown. *B*, detection of cleaved caspase-3 by Western blotting in H9c2 cells treated with $FeSO_4$ (100 μM, up to 24 h). A representative image and quantitative analysis of $n = 3$ experiments are shown. *C* and *D*, pretreatment of neonatal rat cardiomyocytes with 2′-DPD (0.05 and 0.5 mM) attenuated the effect of Lcn2 on the induction of cleaved caspase-3 immunofluorescence (*C*) and immunofluorescent detection of N-terminal Bax (*D*) in a dose-dependent manner. $FeSO_4$ (100 μM, 24 h) was used as positive control (magnification, ×20), and quantitative data (*insets*) represent four experiments ($n = 4$; *, $p < 0.05$, +Lcn2 *versus* −Lcn2 in the absence of 2′-DPD; #, $p < 0.05$, +Lcn2 without 2′-DPD *versus* +Lcn2 with 0.5 mM 2′-DPD).

nism that integrates the ability of Lcn2 to regulate intracellular iron levels with known proapoptotic effects of iron. Although playing a vital role in cellular functions, such as enzyme activity, intracellular iron levels must be carefully regulated because iron, especially ferrous (Fe^{2+}) form, has high potential to cause toxicity. The Haber-Weiss (Fenton) reaction, catalyzed by ferrous iron, generates hydroxyl radicals. Generation of reactive oxygen species is thus one way in which increased intracellular ferrous iron has been proposed to induce apoptosis (54). It was also shown recently that iron enhanced doxorubicin-induced cardiomyocyte apoptosis which was prevented by iron chelation using dexrazoxane, likely via preventing iron-mediated degradation of hypoxia-inducible factors (55). Iron nanoparticles have also been shown to enhance the apoptotic effects of 7-ketocholesterol in cardiomyocytes (56). In general, iron distribution must be

tightly regulated due to the high potential of iron for inducing biological toxicity (57, 58).

Lcn2 has the capability to bind iron, and the complex can internalize through binding to two potential Lcn2 receptors, 24p3R and/or megalin (34, 59). We used PG-SK dye which is quenched by binding iron, especially ferrous form, and showed that Lcn2 treatment of cardiomyocytes resulted in a decrease of PG-SK fluorescence, indicating an increase of intracellular iron pool. We also confirmed that increasing intracellular iron with $FeSO_4$ induced cardiomyocyte apoptosis and that chemical chelation of free intracellular iron attenuated Lcn2-induced caspase-3 activity. This is in keeping with the literature cited above showing an important role for iron in cardiomyocyte apoptosis (54–56). One study suggested that treatment of the atrial derived HL-1 cell line with recombinant enterobactin-Fe^{3+} loaded or iron-free Lcn2 protein showed no apoptosis induction (23). However, it may be that ferrous iron is important in mediating the proapoptotic effects of Lcn2. Interestingly, although the average intracellular iron level increased in the cell population treated by Lcn2, cell by cell image analysis indicated that the effect was more pronounced in a subpopulation of cells. We therefore examined whether individual cells showing the most pronounced increase in intracellular iron showed an increase in cell death. Indeed, decreased PG-SK fluorescence correlated well with cleaved caspase-3 immunoreactivity in individual cells. Because iron has multiple roles in health and disease (57, 58) our observations on a mechanistic role for iron in proapoptotic effects of Lcn2 may have more widespread, and thus far unappreciated, implications in understanding additional physiological effects of Lcn2 (10).

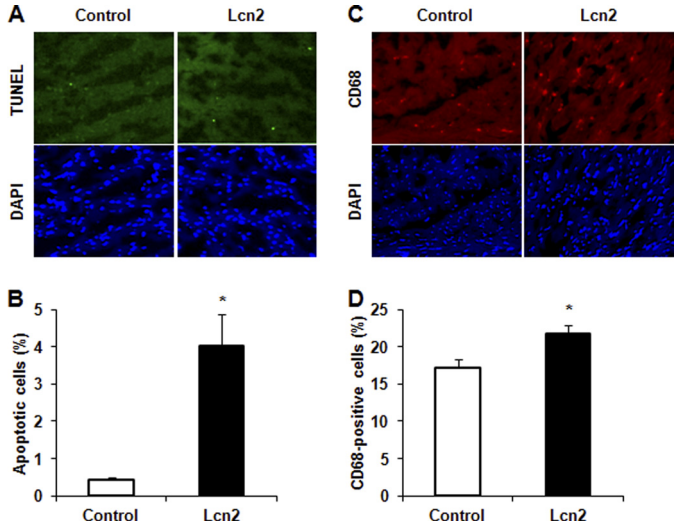

FIGURE 7. **Determination of apoptosis and inflammation in heart section.** *A* and *C*, mouse heart sections were prepared after 14 days of Lcn2 administration, and apoptotic cells were determined using TUNEL assay for DNA fragmentation (*A*) and macrophage infiltration detected by CD68 immunofluorescence (*C*), with cell nuclei stained using DAPI. *B* and *D*, quantitative analysis of multiple field of view of sections from $n = 4$ nice is shown in histogram (*, $p < 0.01$ and 0.05 in *B* and *D*, respectively).

Further investigation of the intracellular mechanisms of Lcn2-induced cardiomyocyte apoptosis demonstrated activation of the intrinsic apoptotic pathway. In particular, we used several approaches to demonstrate Bax translocation to the mitochondrial membrane, a subsequent disruption of mitochondrial membrane potential, and caspase-3 activation. This is in keeping with published work showing that $FeSO_4$ induced mitochondrial damage leading to nuclear DNA condensation and fragmentation (32). It has also been shown that iron induced mitochondrial damage and caused caspase-3 activation, NF-κB induction, and decreased Bcl-2 expression (32). Here, we also confirmed that increasing intracellular iron with $FeSO_4$ induced cardiomyocyte apoptosis and that chemical chelation of free intracellular iron attenuated Lcn2-induced Bax translocation to mitochondria.

To investigate the physiological significance of our observations we then conducted *in vivo* studies in mice administered Lcn2 for 14 days. Good rationale for these studies also comes from the fact that iron accumulation has been identified as an important mediator of age-associated cardiac apoptosis and proposed as an effective pharmacologic target for therapeutic intervention (37). Analysis of TUNEL-positive cells showed a characteristic low value in wild-type mice of <0.5%, but this was significantly increased in animals treated with Lcn2, thus confirming translation of our cell-based studies to an animal model. We analyzed functional parameters in the heart and found that Lcn2 administration tended to induce an unexpected improvement in cardiac function. However, it is important to note that Lcn2 also promotes an acute inflammatory response, as we observed here via CD68 immunofluorescence to monitor macrophage infiltration. It is known that inflammation can induce intracardiac volume depletion, inducing more rapid heart rate and reduced size of cardiac chambers. Additional effects of Lcn2, such as changes in cardiac metabolism, which are still unknown, may also contribute to functional parameters we measured here using echocardiography. Thus, our study indicated an early compensatory stage of cardiac remodeling in the face of elevated apoptosis and inflammation. The temporal nature of cardiac remodeling events is highly significant (5), and this is also likely to be the case for Lcn2-mediated changes. It will be of interest to perform more chronic studies and assess long term changes in cardiac remodeling induced by Lcn2 and whether cardiac iron content is increased in such animals. Indeed, iron overload is known to cause ele-

TABLE 1

Functional parameters derived from echocardiography analysis in hearts from mice treated with Lcn2 or PBS only

Analysis is from six mice and ten mice in control and Lcn2 groups, respectively, and data are presented as mean ± S.E.

Measurement	E′ velocity	Fractional shortening	Cardiac output	Left ventricular volume		Heart rate
				Diastolic	Systolic	
	mm/s	*%*	*ml/min*	*ml*	*ml*	*beats/min*
Control	18.12 ± 0.57	22.43 ± 1.29	12.28 ± 1.12	63.25 ± 2.60	33.40 ± 2.83	393.09 ± 9.29
+Lcn2	24.39 ± 1.26[a]	27.19 ± 1.94[a]	14.73 ± 0.70[a]	64.02 ± 2.25	28.56 ± 2.19	405.86 ± 11.05

[a] $p < 0.05$ (Lcn2 *vs.* control).

vated oxidative stress, myocardial apoptosis, systolic and diastolic dysfunction, and increased morbidity (35, 38, 60).

In conclusion, Lcn2-induced cardiomyocyte apoptosis is at least in part mediated via an increase in intracellular iron levels and induction of the intrinsic mitochondrial pathway via translocation and activation of Bax. Further experiments to understand fully the regulation of various components of cardiac remodeling by Lcn2 and the long term consequences of such changes *in vivo* will now be of great interest.

Acknowledgments—We thank Helen K. W. Law (Institut Pasteur Paris) for discussion and analysis of flow cytometry data.

REFERENCES

1. Mazzone, T., Chait, A., and Plutzky, J. (2008) Cardiovascular disease risk in type 2 diabetes mellitus: insights from mechanistic studies. *Lancet* **371,** 1800–1809
2. Trivedi, P. S., and Barouch, L. A. (2008) Cardiomyocyte apoptosis in animal models of obesity. *Curr. Hypertens. Rep.* **10,** 454–460
3. Walsh, K. (2009) Adipokines, myokines and cardiovascular disease. *Circ. J.* **73,** 13–18
4. Artham, S. M., Lavie, C. J., Patel, H. M., and Ventura, H. O. (2008) Impact of obesity on the risk of heart failure and its prognosis. *J. Cardiometab. Syndr.* **3,** 155–161
5. Abel, E. D., Litwin, S. E., and Sweeney, G. (2008) Cardiac remodeling in obesity. *Physiol. Rev.* **88,** 389–419
6. Schwartz, N., Michaelson, J. S., and Putterman, C. (2007) Lipocalin-2, TWEAK, and other cytokines as urinary biomarkers for lupus nephritis. *Ann. N.Y. Acad. Sci.* **1109,** 265–274
7. Kjeldsen, L., Johnsen, A. H., Sengeløv, H., and Borregaard, N. (1993) Isolation and primary structure of NGAL, a novel protein associated with human neutrophil gelatinase. *J. Biol. Chem.* **268,** 10425–10432
8. Flower, D. R. (1996) The lipocalin protein family: structure and function. *Biochem. J.* **318,** 1–14
9. Cowland, J. B., and Borregaard, N. (1997) Molecular characterization and pattern of tissue expression of the gene for neutrophil gelatinase-associated lipocalin from humans. *Genomics* **45,** 17–23
10. Jang, Y., Lee, J., Wang, Y., and Sweeney, G. (2011) Emerging clinical and experimental evidence for the role of lipocalin-2 in metabolic syndrome. *Clin. Exp. Physiol. Pharmacol.*, in press
11. Wang, Y., Lam, K. S., Kraegen, E. W., Sweeney, G., Zhang, J., Tso, A. W., Chow, W. S., Wat, N. M., Xu, J. Y., Hoo, R. L., and Xu, A. (2007) Lipocalin-2 is an inflammatory marker closely associated with obesity, insulin resistance, and hyperglycemia in humans. *Clin. Chem.* **53,** 34–41
12. Choi, K. M., Lee, J. S., Kim, E. J., Baik, S. H., Seo, H. S., Choi, D. S., Oh, D. J., and Park, C. G. (2008) Implication of lipocalin-2 and visfatin levels in patients with coronary heart disease. *Eur. J. Endocrinol.* **158,** 203–207
13. Law, I. K., Xu, A., Lam, K. S., Berger, T., Mak, T. W., Vanhoutte, P. M., Liu, J. T., Sweeney, G., Zhou, M., Yang, B., and Wang, Y. (2010) Lipocalin-2 deficiency attenuates insulin resistance associated with aging and obesity. *Diabetes* **59,** 872–882
14. Guo, H., Jin, D., Zhang, Y., Wright, W., Bazuine, M., Brockman, D. A., Bernlohr, D. A., and Chen, X. (2010) Lipocalin-2 deficiency impairs thermogenesis and potentiates diet-induced insulin resistance in mice. *Diabetes* **59,** 1376–1385
15. Yan, Q. W., Yang, Q., Mody, N., Graham, T. E., Hsu, C. H., Xu, Z., Houstis, N. E., Kahn, B. B., and Rosen, E. D. (2007) The adipokine lipocalin 2 is regulated by obesity and promotes insulin resistance. *Diabetes* **56,** 2533–2540
16. van Dam, R. M., and Hu, F. B. (2007) Lipocalins and insulin resistance: etiological role of retinol-binding protein 4 and lipocalin-2? *Clin. Chem.* **53,** 5–7
17. Damman, K., van Veldhuisen, D. J., Navis, G., Voors, A. A., and Hillege, H. L. (2008) Urinary neutrophil gelatinase-associated lipocalin (NGAL), a marker of tubular damage, is increased in patients with chronic heart failure. *Eur. J. Heart Fail.* **10,** 997–1000
18. Bolignano, D., Basile, G., Parisi, P., Coppolino, G., Nicocia, G., and Buemi, M. (2009) Increased plasma neutrophil gelatinase-associated lipocalin levels predict mortality in elderly patients with chronic heart failure. *Rejuvenation Res.* **12,** 7–14
19. Poniatowski, B., Malyszko, J., Bachorzewska-Gajewska, H., Malyszko, J. S., and Dobrzycki, S. (2009) Serum neutrophil gelatinase-associated lipocalin as a marker of renal function in patients with chronic heart failure and coronary artery disease. *Kidney Blood Press. Res.* **32,** 77–80
20. Yndestad, A., Landrø, L., Ueland, T., Dahl, C. P., Flo, T. H., Vinge, L. E., Espevik, T., Frøland, S. S., Husberg, C., Christensen, G., Dickstein, K., Kjekshus, J., Øie, E., Gullestad, L., and Aukrust, P. (2009) Increased systemic and myocardial expression of neutrophil gelatinase-associated lipocalin in clinical and experimental heart failure. *Eur. Heart J.* **30,** 1229–1236
21. Hemdahl, A. L., Gabrielsen, A., Zhu, C., Eriksson, P., Hedin, U., Kastrup, J., Thorén, P., and Hansson, G. K. (2006) Expression of neutrophil gelatinase-associated lipocalin in atherosclerosis and myocardial infarction. *Arterioscler. Thromb. Vasc. Biol.* **26,** 136–142
22. Bu, D. X., Hemdahl, A. L., Gabrielsen, A., Fuxe, J., Zhu, C., Eriksson, P., and Yan, Z. Q. (2006) Induction of neutrophil gelatinase-associated lipocalin in vascular injury via activation of nuclear factor-κB. *Am. J. Pathol.* **169,** 2245–2253
23. Aigner, F., Maier, H. T., Schwelberger, H. G., Wallnöfer, E. A., Amberger, A., Obrist, P., Berger, T., Mak, T. W., Maglione, M., Margreiter, R., Schneeberger, S., and Troppmair, J. (2007) Lipocalin-2 regulates the inflammatory response during ischemia and reperfusion of the transplanted heart. *Am. J. Transplant.* **7,** 779–788
24. Olivetti, G., Abbi, R., Quaini, F., Kajstura, J., Cheng, W., Nitahara, J. A., Quaini, E., Di Loreto, C., Beltrami, C. A., Krajewski, S., Reed, J. C., and Anversa, P. (1997) Apoptosis in the failing human heart. *N. Engl. J. Med.* **336,** 1131–1141
25. Takemura, G., and Fujiwara, H. (2004) Role of apoptosis in remodeling after myocardial infarction. *Pharmacol. Ther.* **104,** 1–16
26. Narula, J., Haider, N., Virmani, R., DiSalvo, T. G., Kolodgie, F. D., Hajjar, R. J., Schmidt, U., Semigran, M. J., Dec, G. W., and Khaw, B. A. (1996) Apoptosis in myocytes in end-stage heart failure. *N. Engl. J. Med.* **335,** 1182–1189
27. Narula, J., Kolodgie, F. D., and Virmani, R. (2000) Apoptosis and cardiomyopathy. *Curr. Opin. Cardiol.* **15,** 183–188
28. Devireddy, L. R., Teodoro, J. G., Richard, F. A., and Green, M. R. (2001) Induction of apoptosis by a secreted lipocalin that is transcriptionally regulated by IL-3 deprivation. *Science* **293,** 829–834
29. Lee, S., Park, J. Y., Lee, W. H., Kim, H., Park, H. C., Mori, K., and Suk, K. (2009) Lipocalin-2 is an autocrine mediator of reactive astrocytosis. *J. Neurosci.* **29,** 234–249
30. Bong, J. J., Seol, M. B., Kim, H. H., Han, O., Back, K., and Baik, M. (2004) The 24p3 gene is induced during involution of the mammary gland and induces apoptosis of mammary epithelial cells. *Mol. Cell* **17,** 29–34
31. Zheng, L. T., Lee, S., Yin, G. N., Mori, K., and Suk, K. (2009) Down-regulation of lipocalin 2 contributes to chemoresistance in glioblastoma cells. *J. Neurochem.* **111,** 1238–1251
32. Kooncumchoo, P., Sharma, S., Porter, J., Govitrapong, P., and Ebadi, M. (2006) Coenzyme Q(10) provides neuroprotection in iron-induced apoptosis in dopaminergic neurons. *J. Mol. Neurosci.* **28,** 125–141
33. Velez-Pardo, C., Jimenez Del Rio, M., Verschueren, H., Ebinger, G., and Vauquelin, G. (1997) Dopamine and iron induce apoptosis in PC12 cells. *Pharmacol. Toxicol.* **80,** 76–84
34. Devireddy, L. R., Gazin, C., Zhu, X., and Green, M. R. (2005) A cell-surface receptor for lipocalin 24p3 selectively mediates apoptosis and iron uptake. *Cell* **123,** 1293–1305
35. Oudit, G. Y., Trivieri, M. G., Khaper, N., Husain, T., Wilson, G. J., Liu, P., Sole, M. J., and Backx, P. H. (2004) Taurine supplementation reduces oxidative stress and improves cardiovascular function in an iron-overload murine model. *Circulation* **109,** 1877–1885
36. Whittaker, P., Hines, F. A., Robl, M. G., and Dunkel, V. C. (1996) Histopathological evaluation of liver, pancreas, spleen, and heart from iron-overloaded Sprague-Dawley rats. *Toxicol. Pathol.* **24,** 558–563

37. Arvapalli, R. K., Paturi, S., Laurino, J. P., Katta, A., Kakarla, S. K., Gadde, M. K., Wu, M., Rice, K. M., Walker, E. M., Wehner, P., and Blough, E. R. (2010) Deferasirox decreases age-associated iron accumulation in the aging F344XBN rat heart and liver. *Cardiovasc. Toxicol.* **10,** 108–116
38. Wang, Y., Wu, M., Al-Rousan, R., Liu, H., Fannin, J., Paturi, S., Arvapalli, R. K., Katta, A., Kakarla, S. K., Rice, K. M., Triest, W. E., and Blough, E. R. (2011) Iron-induced cardiac damage: role of apoptosis and deferasirox intervention. *J. Pharmacol. Exp. Ther.* **336,** 56–63
39. Kohgo, Y., Ikuta, K., Ohtake, T., Torimoto, Y., and Kato, J. (2008) Body iron metabolism and pathophysiology of iron overload. *Int. J. Hematol.* **88,** 7–15
40. Bachman, M. A., Miller, V. L., and Weiser, J. N. (2009) Mucosal lipocalin 2 has proinflammatory and iron-sequestering effects in response to bacterial enterobactin. *PLoS Pathog.* **5,** e1000622
41. Schmidt-Ott, K. M., Mori, K., Kalandadze, A., Li, J. Y., Paragas, N., Nicholas, T., Devarajan, P., and Barasch, J. (2006) Neutrophil gelatinase-associated lipocalin-mediated iron traffic in kidney epithelia. *Curr. Opin. Nephrol. Hypertens.* **15,** 442–449
42. Goetz, D. H., Holmes, M. A., Borregaard, N., Bluhm, M. E., Raymond, K. N., and Strong, R. K. (2002) The neutrophil lipocalin NGAL is a bacteriostatic agent that interferes with siderophore-mediated iron acquisition. *Mol. Cell* **10,** 1033–1043
43. Yang, J., Goetz, D., Li, J. Y., Wang, W., Mori, K., Setlik, D., Du, T., Erdjument-Bromage, H., Tempst, P., Strong, R., and Barasch, J. (2002) An iron delivery pathway mediated by a lipocalin. *Mol. Cell* **10,** 1045–1056
44. Palanivel, R., Fang, X., Park, M., Eguchi, M., Pallan, S., De Girolamo, S., Liu, Y., Wang, Y., Xu, A., and Sweeney, G. (2007) Globular and full-length forms of adiponectin mediate specific changes in glucose and fatty acid uptake and metabolism in cardiomyocytes. *Cardiovasc. Res.* **75,** 148–157
45. Deleted in proof
46. Xu, G., Zhou, H., Wang, Q., Auersperg, N., and Peng, C. (2006) Activin receptor-like kinase 7 induces apoptosis through up-regulation of Bax and down-regulation of Xiap in normal and malignant ovarian epithelial cell lines. *Mol. Cancer Res.* **4,** 235–246
47. Deleted in proof
48. Hou, Q., and Hsu, Y. T. (2005) Bax translocates from cytosol to mitochondria in cardiac cells during apoptosis: development of a GFP-Bax-stable H9c2 cell line for apoptosis analysis. *Am. J. Physiol. Heart Circ. Physiol.* **289,** H477–487
49. Petrat, F., Rauen, U., and de Groot, H. (1999) Determination of the chelatable iron pool of isolated rat hepatocytes by digital fluorescence microscopy using the fluorescent probe, phen green SK. *Hepatology* **29,** 1171–1179
50. Shin, E. J., Schram, K., Zheng, X. L., and Sweeney, G. (2009) Leptin attenuates hypoxia/reoxygenation-induced activation of the intrinsic pathway of apoptosis in rat H9c2 cells. *J. Cell. Physiol.* **221,** 490–497
51. Mishra, J., Dent, C., Tarabishi, R., Mitsnefes, M. M., Ma, Q., Kelly, C., Ruff, S. M., Zahedi, K., Shao, M., Bean, J., Mori, K., Barasch, J., and Devarajan, P. (2005) Neutrophil gelatinase-associated lipocalin (NGAL) as a biomarker for acute renal injury after cardiac surgery. *Lancet* **365,** 1231–1238
52. Flo, T. H., Smith, K. D., Sato, S., Rodriguez, D. J., Holmes, M. A., Strong, R. K., Akira, S., and Aderem, A. (2004) Lipocalin 2 mediates an innate immune response to bacterial infection by sequestrating iron. *Nature* **432,** 917–921
53. Chan, Y. R., Liu, J. S., Pociask, D. A., Zheng, M., Mietzner, T. A., Berger, T., Mak, T. W., Clifton, M. C., Strong, R. K., Ray, P., and Kolls, J. K. (2009) Lipocalin 2 is required for pulmonary host defense against *Klebsiella* infection. *J. Immunol.* **182,** 4947–4956
54. Munoz, J. P., Chiong, M., García, L., Troncoso, R., Toro, B., Pedrozo, Z., Diaz-Elizondo, J., Salas, D., Parra, V., Núñez, M. T., Hidalgo, C., and Lavandero, S. (2010) Iron induces protection and necrosis in cultured cardiomyocytes: role of reactive oxygen species and nitric oxide. *Free Radic. Biol. Med.* **48,** 526–534
55. Spagnuolo, R. D., Recalcati, S., Tacchini, L., and Cairo, G. (2011) Role of hypoxia-inducible factors in the dexrazoxane-mediated protection of cardiomyocytes from doxorubicin-induced toxicity. *Br. J. Pharmacol.* **163,** 299–312
56. Kahn, E., Baarine, M., Pelloux, S., Riedinger, J. M., Frouin, F., Tourneur, Y., and Lizard, G. (2010) Iron nanoparticles increase 7-ketocholesterol-induced cell death, inflammation, and oxidation on murine cardiac HL1-NB cells. *Int. J. Nanomedicine* **5,** 185–195
57. Goswami, T., Rolfs, A., and Hediger, M. A. (2002) Iron transport: emerging roles in health and disease. *Biochem. Cell Biol.* **80,** 679–689
58. Deleted in proof
59. Hvidberg, V., Jacobsen, C., Strong, R. K., Cowland, J. B., Moestrup, S. K., and Borregaard, N. (2005) The endocytic receptor megalin binds the iron transporting neutrophil-gelatinase-associated lipocalin with high affinity and mediates its cellular uptake. *FEBS Lett.* **579,** 773–777
60. Borgna-Pignatti, C., Cappellini, M. D., De Stefano, P., Del Vecchio, G. C., Forni, G. L., Gamberini, M. R., Ghilardi, R., Piga, A., Romeo, M. A., Zhao, H., and Cnaan, A. (2006) Cardiac morbidity and mortality in deferoxamine- or deferiprone-treated patients with thalassemia major. *Blood* **107,** 3733–3737